

# EM-based Algorithm for Unsupervised Clustering of Measurements from a Radar Sensor Network

Linjie Yan, Pia Addabbo, *Senior Member, IEEE*, Nicomino Fiscante, Carmine Clemente, *Senior Member, IEEE*, Chengpeng Hao, *Senior Member, IEEE*, Gaetano Giunta, *Senior Member, IEEE*, and Danilo Orlando, *Senior Member, IEEE*

**Abstract**—This paper deals with the problem of clustering data returned by a radar sensor network that monitors a region where multiple moving targets are present. The network is formed by nodes with limited functionalities that transmit the estimates of target positions (after a detection) to a fusion center without any association between measurements and targets. To solve the problem at hand, we resort to model-based learning algorithms and instead of applying the plain maximum likelihood approach, due to the related computational requirements, we exploit the latent variable model coupled with the expectation-maximization algorithm. The devised estimation procedure returns posterior probabilities that are used to cluster the huge amount of data collected by the fusion center. Remarkably, we also consider challenging scenarios with an unknown number of targets and estimate it by means of the model order selection rules. The clustering performance of the proposed strategy is compared to that of conventional data-driven methods over synthetic data. The numerical examples point out that the herein proposed solutions can provide reliable clustering performance overcoming the considered competitors.

**Index Terms**—Batch algorithms, expectation-maximization, measurement clustering, multiple moving targets, radar, sensor network, unsupervised learning.

## I. INTRODUCTION

**I**N the recent years, the increase of computational resources has heavily promoted the development and the implementation of sophisticated signal processing techniques in real radar systems. More importantly, with the advent of the big data era, statistical signal processing algorithms have been incorporated into a wider class called “Machine Learning” that has become more and more popular over the years [1], [2] and also comprises deep learning techniques. Two main design

approaches can be identified within this wide class: data-driven and model-based oriented designs. The former operates through a learning stage that relies on training data, namely a set of input-output pairs used to learn the algorithm from the available data, whereas the latter relies on a model grounded on the first physics principles. In both cases, the exploitation of high performance boards becomes unavoidable to fulfill the tight (time) requirements of real radar systems. The methods devised in this paper are framed in the model-based class.

In parallel with the technological advancements, the operating scenarios have become more and more challenging as well as the corresponding estimation/optimization problems. A related example is represented by scenarios where swarms of (possibly noncooperative) targets are moving in the region of interest that is monitored by a network of passive/active radars [3]–[12]. As a matter of fact, the advantages arising from the use of a sensor network are well-known and we mention here the spatial diversity and the energy integration. For this reason, in modern radar systems, the cooperation between systems distributed over the region under surveillance becomes a key factor to improve the reliability of the entire surveillance system. For instance, with focus on ground radars, the spatial diversity of the sensor network can be exploited to face deception/saturation jamming techniques such as range gate stealing [13], [14], that generate false targets to make the radar lose range track on the target.

However, radar networks require special attention in handling a huge amount of data provided by each node, especially in the presence of multiple moving targets [15]–[17]. In this case, the detection can be either centralized or decentralized. In centralized detection, sending raw observations from radar sensors to the fusion center (FC), where the final decision process takes place, imposes a large communication burden. On the other hand, in decentralized detection, radar sensors take their local decisions on the presence of prospective targets and, then, transmit the results of such decisions (compressed data) to the FC. In this case, the amount of transmitted data is lower than in the previous configuration with a consequent energy saving but at the price of performance loss. As a matter of fact, the overall system does not take advantage of diversity. The design of optimized decentralized detector network, which entails the design of both optimal local detectors and fusion rules at FC, does not represent an easy task [18] and some strategies to solve this difficult problem have been proposed in the past [19]–[21]. Moreover, in radar networks, the tracking of multiple targets represents a very

This work was supported in part by the National Natural Science Foundation of China under Grants no. 62201564 and 61971412.

Linjie Yan and Chengpeng Hao are with the Institute of Acoustics, Chinese Academy of Sciences, Beijing, 100190, China. E-mail: yanlinjie16@163.com; haochengp@mail.ioa.ac.cn.

Pia Addabbo is with Università degli Studi “Giustino Fortunato”, viale Raffale Delcogliano, 12, 82100 Benevento, Italy. E-mail: p.addabbo@unifortunato.eu

Nicomino Fiscante and Gaetano Giunta are with Industrial, Electronic and Mechanical Engineering Department, University of Roma Tre, 00146 Rome, Italy. E-mail: nicomino.fiscante@virgilio.it; gaetano.giunta@uniroma3.it.

Carmine Clemente is with the University of Strathclyde, Department of Electronic and Electrical Engineering, 204 George Street, G1 1XW, Glasgow, Scotland. E-mail: carmine.clemente@strath.ac.uk

Daniilo Orlando is with the Engineering Department of Università degli Studi “Niccolò Cusano”, via Don Carlo Gnocchi 3, 00166 Roma, Italy. E-mail: daniilo.orlando@unicusano.it.

challenging problem due to the limited data computational capacity of the FC as well as of the transmit energy of each radar [21]–[24]. Generally speaking, this implies the necessity of using sophisticated (centralized or decentralized) fusion methods [25]–[28]. Anyway, the implementation of centralized fusion methods is computationally expensive [25]. Nevertheless, a preliminary stage that preprocesses and clusters the received observations into homogeneous measurement sets, might reduce the computational load at the FC [29]

Clustering algorithms have been also applied for the design of CFAR and/or selective/robust detectors [30], [31]. Particularly, in [30], received data are transformed to generate specific features based upon the maximal invariant statistic [32] for that problem. Then, such features are clustered in a two-dimensional plane to come up with a detector that is invariant to the disturbance parameters and, hence, can guarantee the constant false alarm rate property. Another design methodology, based on the previous approach, is proposed in [31], where sub-optimal strategies with low complexity have been developed. The expectation-maximization (EM) algorithm is also used for clustering data that can be modeled as a Gaussian Mixture [1]. In particular, in the context of radar systems, the EM algorithm is used to partition clutter returns based upon their spectral properties [33]. To this end, fictitious hidden random variables are introduced to represent the clutter type of each range bin. Interestingly, the classification algorithms have been devised by accounting for different models of the clutter covariance matrix. Whereas, in [34], joint detection and classification architectures have been proposed by extending the work of [33] to the case where an unknown number of multiple point-like targets are present in the region of interest. In [35], the EM algorithm is still used for the target detection in heterogeneous clutter scenarios.

In this paper, we provide a solution to the problem of handling multiple targets in a scene. Actually, this issue is getting more and more critical with the growing number of scenarios in which multiple targets need to be monitored in crowded spaces. As a matter of fact, conventional radar scenarios are getting more densely populated with the arrival of new classes of targets such as unmanned/autonomous vehicles (either in air, land, or sea). The same remark also holds for less conventional but equally challenging radar scenarios such as monitoring space targets. Therefore, we focus on a radar sensor network whose monostatic nodes illuminate the same region of interest where an unknown number of targets are moving. Each node does not perform any association between the measurements related to a detection and the detected targets, and sends to the FC the position estimates corresponding to each detection within a common observation time window. At the design stage, we assume that measurements are collected over a time interval such that the target trajectories can be approximated as straight lines (with a not necessarily constant velocity). Assuming a specific distribution for the measurement noise, we exploit the likelihood function of data to solve the clustering problem. In this respect, we do not resort to the maximum likelihood principle, because it requires the evaluation of the joint likelihood function for each partition of the entire measurement set and targets' number. It

is clear that such a task is unacceptable from a computational standpoint and, more importantly, the maximum likelihood approach would return estimates corresponding to the maximum allowed model order since the likelihood function monotonically increases with the number of unknown parameters [36], [37]. Therefore, to circumvent the above limitations, we introduce fictitious and unobserved discrete random variables that represent target labels associated with the measurements gathered by the FC. Then, exploiting the joint distribution of measurements and the hidden labels, we develop an estimation procedure grounded on the EM algorithm [38] that allows us to obtain a nondecreasing sequence of likelihood values as well as closed-form expressions for the updates of the estimates. The clusters are formed by applying the maximum a posteriori rule, whereas an estimate of the number of targets is returned through the Model Order Selection (MOS) rules [36], [37], [39]–[41].

The performance analysis is carried out over synthetic data and starts from the case where the number of targets is known to proceed with the case where the latter is unknown. As terms of comparison, we consider two conventional data-driven algorithms. The numerical examples show the superiority of the proposed approach over the considered competitors in classifying the collected measurements.

The remainder of this paper is organized as follows. In the next section, we describe the surveillance system and provide a formal statement of the problem. In Section III, we devise the EM-based estimation procedure when the number of targets is known, whereas in Section IV we extend such a procedure to the case of an unknown number of targets. The numerical examples are contained in Section V and, finally, concluding remarks along with the description of possible future research lines are confined to Section VI.

### A. Notation

In the sequel, vectors are denoted by boldface lower-case. As to numerical sets,  $\mathbb{N}$  is the set of natural numbers,  $\mathbb{R}$  is the set of real numbers, and  $\mathbb{R}^{N \times M}$  is the Euclidean space of  $(N \times M)$ -dimensional real matrices (or vectors if  $M = 1$ ). The Cartesian product of two sets  $A$  and  $B$  is denoted by  $A \times B$ . The acronyms PDF and PMF stand for Probability Density Function and Probability Mass Function, respectively, whereas the conditional pdf of a random variable  $x$  given another random variable  $y$  is denoted by  $f(x|y)$ . The probability of an event  $\mathcal{A}$  is defined as  $P\{\mathcal{A}\}$ , whereas the conditional probability of  $\mathcal{A}$  given another event  $\mathcal{B}$  is  $P\{\mathcal{A}|\mathcal{B}\}$ . Symbol  $\lfloor \cdot \rfloor$  represents the highest integer lower than the argument while  $|x|$  is the absolute value of  $x \in \mathbb{R}$ . Finally, we write  $x \sim \mathcal{N}(m, \sigma^2)$  if  $x$  is a Gaussian random variable with mean  $m$  and variance  $\sigma^2 > 0$ .

## II. SIGNAL MODEL AND PROBLEM FORMULATION

Let us consider a sensor network of  $K \in \mathbb{N}$  monostatic radars deployed to illuminate the same region of interest. The capabilities of such systems are limited to target detection and rough estimation of its range and azimuth. Assuming that the region of interest is populated by an unknown number,  $L$



In the next section, we design an estimation procedure to solve problem (5) and, as a byproduct, (6), grounded on the EM-algorithm. Then, in Section IV, we address the case where  $L$  is unknown.

### III. ESTIMATION PROCEDURE FOR KNOWN NUMBER OF TARGETS

From a mathematical point of view, the plain maximization in (5) is a difficult task at least to the best of authors' knowledge. For this reason, we resort to the EM-algorithm that is an iterative procedure with closed-form updates for the estimates of interest and provides at least a local maximum [1], [38], [43]. The EM-algorithm repeats two steps called E-step and M-step until a stopping criterion is not satisfied. The former consists in updating the a posteriori probability of the event  $c_n = l$  given the  $n$ th measurement  $y_n$  whereas in the latter step, the log-likelihood function is maximized to obtain updated parameter estimates.

Thus, let us start from the E-step and denote by  $\hat{\boldsymbol{\theta}}^{(h-1)}$  and  $\hat{\pi}_l^{(h-1)}$ ,  $l \in \mathcal{A}$ , the estimates of  $\boldsymbol{\theta}$  and  $\pi_l$ ,  $l \in \mathcal{A}$ , at the  $(h-1)$ th iteration, respectively. The E-step leads to the computation of

$$\begin{aligned} p_n^{(h-1)}(l) &= P \left\{ c_n = l | y_n; \hat{\boldsymbol{\theta}}^{(h-1)}, \hat{\pi}_l^{(h-1)} \right\} \\ &= \frac{f(y_n | c_n = l; \hat{\boldsymbol{\theta}}^{(h-1)}) \hat{\pi}_l^{(h-1)}}{\sum_{\bar{l} \in \mathcal{A}} f(y_n | c_n = \bar{l}; \hat{\boldsymbol{\theta}}^{(h-1)}) \hat{\pi}_{\bar{l}}^{(h-1)}} \end{aligned} \quad (7)$$

for  $l \in \mathcal{A}$  and  $n = 1, \dots, N$ . As for the M-step, after applying the Jensen inequality to the argument of (5), we come up with the following optimization problem

$$\max_{\boldsymbol{\theta}} \sum_{n=1}^N \sum_{l \in \mathcal{A}} p_n^{(h-1)}(l) \log \left( \frac{f(y_n | c_n = l; \boldsymbol{\theta}) \pi_l}{p_n^{(h-1)}(l)} \right), \quad (8)$$

where

$$f(y_n | c_n = l; \boldsymbol{\theta}) = \frac{\exp \left[ -\frac{1}{2\sigma_l^2} (y_n - a_l x_n - b_l)^2 \right]}{\sqrt{2\pi\sigma_l}}. \quad (9)$$

Problem (8) is tantamount to

$$\max_{\boldsymbol{\theta}} \sum_{n=1}^N \sum_{l \in \mathcal{A}} \left[ p_n^{(h-1)}(l) \log[f(y_n | c_n = l; \boldsymbol{\theta})] + p_n^{(h-1)}(l) \log(\pi_l) \right]. \quad (10)$$

Thus, the maximization over  $\pi_l$ ,  $l \in \mathcal{A}$ , can be accomplished by solving

$$\begin{cases} \max_{\pi_l, l \in \mathcal{A}} \sum_{n=1}^N \sum_{l \in \mathcal{A}} p_n^{(h-1)}(l) \log(\pi_l), \\ \text{subject to} \quad \sum_{l \in \mathcal{A}} \pi_l = 1. \end{cases} \quad (11)$$

According to the method of Lagrange multipliers, we set to zero the first derivative with respect to the unknowns of the Lagrangian function whose expression is

$$\sum_{n=1}^N \sum_{l \in \mathcal{A}} p_n^{(h-1)}(l) \log(\pi_l) - \lambda \left( \sum_{l \in \mathcal{A}} \pi_l - 1 \right), \quad (12)$$

where  $\lambda$  is the Lagrange multiplier. Proceeding in this way, we obtain that

$$\begin{aligned} \sum_{n=1}^N p_n^{(h-1)}(l) \frac{1}{\pi_l} - \lambda &= 0 \\ \implies \pi_l &= \frac{1}{\lambda} \sum_{n=1}^N p_n^{(h-1)}(l), \quad l \in \mathcal{A}. \end{aligned} \quad (13)$$

Considering the constraint leads to

$$\begin{aligned} \frac{1}{\lambda} \sum_{l \in \mathcal{A}} \sum_{n=1}^N p_n^{(h-1)}(l) &= 1 \\ \implies \lambda &= \sum_{n=1}^N \sum_{l \in \mathcal{A}} p_n^{(h-1)}(l) = N \end{aligned} \quad (14)$$

and, hence,

$$\pi_l^{(h)} = \frac{1}{N} \sum_{n=1}^N p_n^{(h-1)}(l), \quad l \in \mathcal{A}. \quad (15)$$

It still remains to maximize the objective function with respect to the other parameters. Thus, neglecting the irrelevant constants, the optimization problem to be solved can be formulated as

$$\max_{\boldsymbol{\theta}} g(\boldsymbol{\theta}), \quad (16)$$

where

$$\begin{aligned} g(\boldsymbol{\theta}) &= \sum_{n=1}^N \sum_{l \in \mathcal{A}} p_n^{(h-1)}(l) \\ &\times \left[ -\frac{1}{2} \log(2\pi\sigma_l^2) - \frac{1}{2\sigma_l^2} (y_n - a_l x_n - b_l)^2 \right]. \end{aligned} \quad (17)$$

Focusing on  $\sigma_l^2$ ,  $l \in \mathcal{A}$ , we firstly notice that  $\forall l \in \mathcal{A}$

$$\lim_{\sigma_l^2 \rightarrow +\infty} g(\boldsymbol{\theta}) = -\infty \quad \text{and} \quad \lim_{\sigma_l^2 \rightarrow 0} g(\boldsymbol{\theta}) = -\infty. \quad (18)$$

Thus, the maximum over  $\sigma_l^2$  can be found by setting to zero the first derivative of  $g(\boldsymbol{\theta})$  with respect to  $\sigma_l^2$ , namely

$$\sum_{n=1}^N p_n^{(h-1)}(l) \left[ -\frac{1}{2\sigma_l^2} + \frac{1}{2(\sigma_l^2)^2} (y_n - a_l x_n - b_l)^2 \right] = 0 \quad (19)$$

and solving with respect to  $\sigma_l^2$  we obtain

$$\tilde{\sigma}_l^2 = \frac{\sum_{n=1}^N (y_n - a_l x_n - b_l)^2 p_n^{(h-1)}(l)}{\sum_{n=1}^N p_n^{(h-1)}(l)}, \quad l \in \mathcal{A} \quad (20)$$

Moreover, when  $\sigma_l^2 < (\tilde{\sigma}_l^2)^{(h)}$ , the derivative is positive (increasing function), whereas for  $\sigma_l^2 > (\tilde{\sigma}_l^2)^{(h)}$ , the derivative is negative (decreasing function). Replacing (20) in (17)

and neglecting the terms that do not enter the optimization problem, the latter is equivalent to

$$\min_{\substack{a_l, b_l \\ l \in \mathcal{A}}} \sum_{l \in \mathcal{A}} g(a_l, b_l), \quad (21)$$

where

$$g(a_l, b_l) = \left( \sum_{n=1}^N p_n^{(h-1)}(l) \right) \times \log \left[ \sum_{n=1}^N (y_n - a_l x_n - b_l)^2 p_n^{(h-1)}(l) \right]. \quad (22)$$

Let us study the behavior of  $g(a_l, b_l)$  at the endpoints of its domain. To this end, it is not difficult to show that

$$\lim_{\substack{|a_l| \rightarrow +\infty \\ |b_l| \rightarrow +\infty}} g(a_l, b_l) = +\infty, \quad l \in \mathcal{A}. \quad (23)$$

Therefore, we set to zero the first derivative over  $a_l$  of  $g(a_l, b_l)$  to obtain

$$\left( \sum_{n=1}^N p_n^{(h-1)}(l) \right) \frac{1}{\sum_{n=1}^N (y_n - a_l x_n - b_l)^2 p_n^{(h-1)}(l)} \times \left[ \sum_{n=1}^N p_n^{(h-1)}(l) 2(y_n - a_l x_n - b_l)(-x_n) \right] = 0 \quad (24)$$

and, hence,

$$\tilde{a}_l = \frac{\sum_{n=1}^N p_n^{(h-1)}(l)(y_n - b_l)x_n}{\sum_{n=1}^N p_n^{(h-1)}(l)x_n^2}, \quad l \in \mathcal{A}. \quad (25)$$

Replacing (25) into (22) and neglecting the irrelevant constants, we can consider

$$\min_{b_l} \log g_1(b_l), \quad (26)$$

where

$$g_1(b_l) = \sum_{n=1}^N \left\{ \frac{p_n^{(h-1)}(l)}{(B_l^{(h-1)})^2} \left[ y_n B_l^{(h-1)} - x_n \sum_{\bar{n}=1}^N p_{\bar{n}}^{(h-1)}(l) y_{\bar{n}} x_{\bar{n}} + b_l (x_n A_l^{(h-1)} - B_l^{(h-1)}) \right]^2 \right\}, \quad (27)$$

with

$$A_l^{(h-1)} = \sum_{\bar{n}=1}^N p_{\bar{n}}^{(h-1)}(l) x_{\bar{n}}, \quad (28)$$

$$B_l^{(h-1)} = \sum_{\bar{n}=1}^N p_{\bar{n}}^{(h-1)}(l) x_{\bar{n}}^2.$$

Now, setting to zero the first derivative of  $\log g_1(b_l)$  with respect to  $b_l$  leads to

$$\frac{1}{g_1(b_l)} \sum_{n=1}^N \frac{2p_n^{(h-1)}(l)}{B_l^{(h-1)}} \left[ y_n B_l^{(h-1)} - x_n \sum_{\bar{n}=1}^N p_{\bar{n}}^{(h-1)}(l) y_{\bar{n}} x_{\bar{n}} + b_l (x_n A_l^{(h-1)} - B_l^{(h-1)}) \right] \times \left( \frac{x_n A_l^{(h-1)} - B_l^{(h-1)}}{B_l^{(h-1)}} \right) = 0, \quad (29)$$

and, as a consequence, the estimate update for  $b_l$  is given by

$$\hat{b}_l^{(h)} = \frac{1}{\sum_{n=1}^N p_n^{(h-1)}(l) (x_n A_l^{(h-1)} - B_l^{(h-1)})^2} \times \left\{ \sum_{n=1}^N \left[ p_n^{(h-1)}(l) x_n (x_n A_l^{(h-1)} - B_l^{(h-1)}) \right] \times \sum_{\bar{n}=1}^N p_{\bar{n}}^{(h-1)}(l) y_{\bar{n}} x_{\bar{n}} - \sum_{n=1}^N \left[ p_n^{(h-1)}(l) y_n \times (x_n A_l^{(h-1)} - B_l^{(h-1)}) \sum_{\bar{n}=1}^N p_{\bar{n}}^{(h-1)}(l) x_{\bar{n}}^2 \right] \right\}. \quad (30)$$

Finally, the updates for the estimates of  $a_l$  and  $\sigma_l^2$  can be written as

$$\hat{a}_l^{(h)} = \frac{\sum_{n=1}^N p_n^{(h-1)}(l) (y_n - \hat{b}_l^{(h)}) x_n}{\sum_{n=1}^N p_n^{(h-1)}(l) x_n^2}, \quad l \in \mathcal{A}. \quad (31)$$

and

$$(\hat{\sigma}_l^2)^{(h)} = \frac{\sum_{n=1}^N (y_n - \hat{a}_l^{(h)} x_n - \hat{b}_l^{(h)})^2 p_n^{(h-1)}(l)}{\sum_{n=1}^N p_n^{(h-1)}(l)}, \quad l \in \mathcal{A}, \quad (32)$$

respectively.

Summarizing, the E-step given by (7) and the above updates obtained from the M-step are repeated until a stopping criterion is not satisfied. Specifically, the iterations end when

$$\Delta \mathcal{L}(h) = \left| \left[ \mathcal{L} \left( y_1, \dots, y_N; \hat{\boldsymbol{\theta}}^{(h)}, \hat{\pi}_1^{(h)}, \dots, \hat{\pi}_L^{(h)} \right) - \mathcal{L} \left( y_1, \dots, y_N; \hat{\boldsymbol{\theta}}^{(h-1)}, \hat{\pi}_1^{(h-1)}, \dots, \hat{\pi}_L^{(h-1)} \right) \right] \right| / \left| \mathcal{L} \left( y_1, \dots, y_N; \hat{\boldsymbol{\theta}}^{(h)}, \hat{\pi}_1^{(h)}, \dots, \hat{\pi}_L^{(h)} \right) \right| < \epsilon, \quad (33)$$

where  $\epsilon > 0$  and

$$\mathcal{L} \left( y_1, \dots, y_N; \hat{\boldsymbol{\theta}}^{(h)}, \hat{\pi}_1^{(h)}, \dots, \hat{\pi}_L^{(h)} \right) = \sum_{n=1}^N \log \left[ \sum_{l \in \mathcal{A}} f \left( y_n | c_n = l; \hat{\boldsymbol{\theta}}^{(h)} \right) \pi_l^{(h)} \right], \quad (34)$$

or after a maximum number of iterations denoted by  $h_{max}$ .

In the next section, we show how to incorporate the estimates obtained through the EM-algorithm into the MOS rules to determine the number of targets  $L$ .

#### IV. ESTIMATION PROCEDURE FOR UNKNOWN NUMBER OF TARGETS

The estimation of the number of targets relies on the MOS rules since the hypotheses corresponding to scenarios with different numbers of targets are nested. As stated in Section I, the maximum likelihood approach experiences an overestimation of the parameter space size [37], [44] and, hence, a penalty term is required to balance the corresponding growth of the likelihood function. In what follows, we consider the Akaike Information Criterion (AIC), the Bayesian Information Criterion (BIC), and the Generalized Information Criterion (GIC) [37], whose general structure is

$$\hat{L} = \arg \min_{L \in \{1, \dots, L_{\max}\}} \left\{ -2\mathcal{L}\left(y_1, \dots, y_N; \hat{\boldsymbol{\theta}}^{(h_L)}, \hat{\pi}_1^{(h_L)}, \dots, \hat{\pi}_L^{(h_L)}\right) + p(L) \right\}, \quad (35)$$

where  $h_L$  is the number of iterations used by the EM-based estimation procedure introduced in Section III assuming  $L$  targets and  $p(L)$  is a penalty term defined as follows

$$p(L) = \begin{cases} 2n_p(L), & \text{AIC,} \\ (1 + \rho)n_p(L), \quad \rho \geq 1, & \text{GIC,} \\ n_p(L) \log(N), & \text{BIC,} \end{cases} \quad (36)$$

with  $n_p(L) = 4L$  being the number of unknown parameters in the presence of  $L$  targets.

Once  $\hat{L}$  is computed through (35), we can define  $\hat{\mathcal{A}} = \{1, \dots, \hat{L}\}$  and the association rule (6) becomes

$$\hat{l} = \arg \max_{l \in \hat{\mathcal{A}}} P \left\{ c_n = l | y_n; \hat{\boldsymbol{\theta}}^{(h_{\hat{L}})}, \hat{\pi}_l^{(h_{\hat{L}})} \right\}, \quad (37)$$

where  $\hat{\boldsymbol{\theta}}^{(h_{\hat{L}})}$  and  $\hat{\pi}_l^{(h_{\hat{L}})}$ ,  $l \in \hat{\mathcal{A}}$ , are the estimates corresponding to the case  $L = \hat{L}$ .

#### V. NUMERICAL EXAMPLES AND DISCUSSION

In this section, we provide illustrative examples aimed at assessing the classification/clustering performance of the proposed approach by resorting to Monte Carlo (MC) counting techniques. Specifically, we start the analysis by assuming that  $L$  is known and consider two operating scenarios with  $L = 5$  and  $L = 10$  targets. Then, we focus on the estimation capabilities for the number of targets by setting  $L_{\max} = 10$  and the actual value of  $L$  equal to 3 and 7.

In each scenario, we directly generate the trajectories of multiple targets in Cartesian coordinates with the number of measurements for the  $l$ th target,  $N_l$  say,  $l = 1, \dots, L$ ,<sup>1</sup> being a uniformly distributed random variable in [60, 90]. In

<sup>1</sup>Notice that the constraint  $\sum_{l=1}^L N_l = N$  holds.

---

#### Algorithm 1: Initialization of $a_l$ and $b_l$ .

---

**Input:**  $L, y_n, x_n, n = 1, \dots, N$

**Output:**  $a_l, b_l, l = 1, \dots, L$

**Initialization:** set  $N'_1 = N, y_{n'_1} = y_n, x_{n'_1} = x_n, n'_1 = n = 1, \dots, N$

**for**  $l = 1, \dots, L$  **do**

1. compute  $a_l$  and  $b_l$  of the linear regression by

$$a_l = \left( \frac{\sum_{n'_1=1}^{N'_1} (x_{n'_1} - \bar{x})(y_{n'_1} - \bar{y})}{\sum_{n'_1=1}^{N'_1} (x_{n'_1} - \bar{x})^2} \right)$$

and  $b_l = \bar{y} - a_l \bar{x}$  using  $N'_l$  measurements with  $\bar{x}$  and  $\bar{y}$  the mean value of  $x_{n'_1}$  and  $y_{n'_1}$ , respectively;

2. compute the standard deviation of  $(x_{n'_1}, y_{n'_1})$

with respect to the fitted line, namely,

$$d_l(n'_1) = |y_{n'_1} - a_l x_{n'_1} - b_l| / \sqrt{a_l^2 + b_l^2},$$

$n'_1 = 1, \dots, N'_l$ ;

3. set  $l = l + 1$ ;

4. select the  $\lfloor N/L \rfloor$  measurements with the minimum  $d_l(n'_1)$  and discard them, we have

$$N'_l = N'_{l-1} - \lfloor N/L \rfloor;$$

5. go to step 1 using the remaining measurements until the loop ends.

**end**

---

addition, trajectory intersections are included in the considered scenarios making the classification task more challenging.

For comparison purposes, we compare the proposed approach with two classical machine learning clustering techniques, namely the K-Nearest-Neighbor (KNN) and K-means [1], [45], [46]. The former is a supervised method, whereas the latter is unsupervised. In the ensuing examples, we assume that the ratio between the quantity of training and validation data for the KNN is 4/6 and the number of nearest neighbors is 50.

As for the initialization of the EM-based procedure, we set  $\pi_l = 1/L, l = 1, \dots, L$ , while the initial values of  $a_l$  and  $b_l$  are computed by means of an *ad hoc* strategy summarized in Algorithm 1. Possible initial values the noise variances are

$$\sigma_l^2 = \sum_{n'_1=1}^{N'_1} (y_{n'_1} - a_l x_{n'_1} - b_l)^2 / N'_1, \quad l \in \mathcal{A}, \quad (38)$$

where  $N'_l$  denotes the number of measurements used to compute the initial trajectory coefficients of the  $l$ th target in Algorithm 1.

In each scenario, the measurements are affected by an uncertainty with variance  $\sigma_l^2 = 50, l = 1, \dots, L$  that lead to a significant “mix” of the targets’ measurements. Finally, we anticipate here that, in order to achieve a satisfactory compromise between convergence and computational load,  $\epsilon$  is set to  $10^{-5}$  and  $h_{max}$  is set to 150 and 250 for  $L = 5$  and  $L = 10$ , respectively, as corroborated by the subsequent convergence analysis.

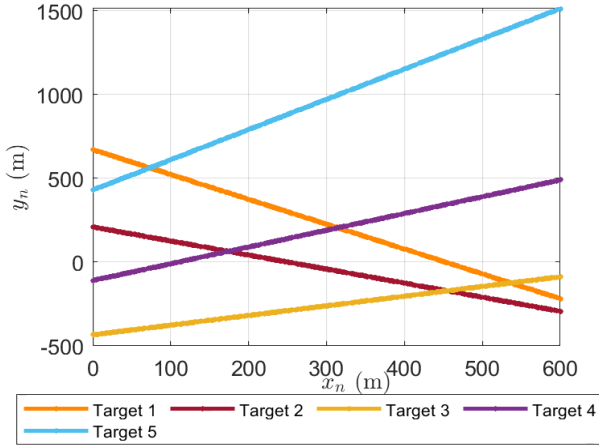


Fig. 2: Clean target trajectories without measurement noise (first scenario).

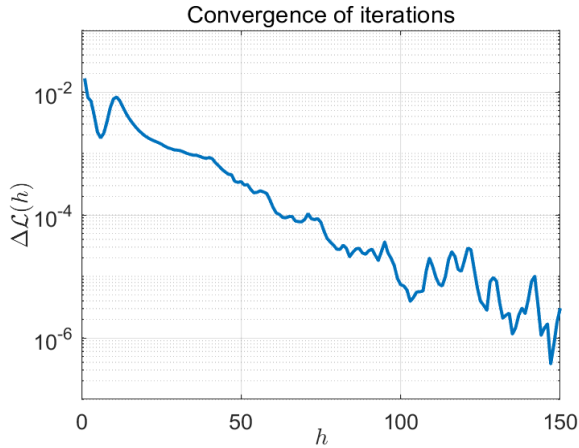


Fig. 3:  $\Delta\mathcal{L}(h)$  versus  $h$  for the EM-based procedure (first scenario).

#### A. First Operating Scenario for Known Number of Targets $L = 5$

In this scenario, we consider five targets whose measurements are generated as follows

- **Target 1:**  $y_{n_1}|c_{n_1} = 1 \sim \mathcal{N}(-1.4826x_{n_1} + 671, \sigma_1^2)$ ,  $n_1 = 1, \dots, N_1$ ;
- **Target 2:**  $y_{n_2}|c_{n_2} = 2 \sim \mathcal{N}(-0.8391x_{n_2} + 310, \sigma_2^2)$ ,  $n_2 = 1, \dots, N_2$ ;
- **Target 3:**  $y_{n_3}|c_{n_3} = 3 \sim \mathcal{N}(0.5774x_{n_3} - 434, \sigma_3^2)$ ,  $n_3 = 1, \dots, N_3$ ;
- **Target 4:**  $y_{n_4}|c_{n_4} = 4 \sim \mathcal{N}(x_{n_4} - 110, \sigma_4^2)$ ,  $n_4 = 1, \dots, N_4$ ;
- **Target 5:**  $y_{n_5}|c_{n_5} = 5 \sim \mathcal{N}(1.8040x_{n_5} + 430, \sigma_5^2)$ ,  $n_5 = 1, \dots, N_5$ ;

where  $x_{n_l}$ ,  $l = 1, \dots, L$ , are generated by randomly selecting integers from 1 to  $N$ . The above target trajectories without measurement noise are shown in Figure 2.

In Figure 3, we plot the curves of  $\Delta\mathcal{L}(h)$  averaged over 1000 independent trials to select a suitable value for  $h_{max}$ . It can be seen that the relative variation of the log-likelihood

function is lower than  $10^{-5}$  after 150 iterations and, hence, for this scenario, we set  $h_{max} = 150$ .

The classification capabilities of the proposed architecture in comparison with the two considered competitors are investigated in Figures 4-6. Specifically, the true clusters and the classification results over a single MC trial are shown in Figure 4. The inspection of this figure clearly points out the superiority of the proposed method in measurement labeling over the counterparts. As a matter of fact, from a qualitative point of view, both KNN and K-means experience evident misclassification errors due to the association of measurements to wrong targets. As a consequence, the trajectory of a given target appears divided into segments corresponding to different targets. This kind of segmentation is more evident in Subfigure 4(d) that reports the classification results of K-means. Moreover, Subfigure 4(b) contains the target trajectories, obtained through the estimates of  $a_l$  and  $b_l$ ,  $l = 1, \dots, L$ , that<sup>2</sup> perfectly fit with the measurements (at least for the considered parameter setting).

Figure 5 shows the mean classification consistency (%), which is defined as the ratio between the number of correct classifications over the true target categories averaged over 1000 independent trials. It turns out that the proposed EM-based classifier achieves a classification gain of approximately 12.6% and 59% with respect to the KNN and K-means, respectively. Figure 6 shows the mean classification error (%) averaged over 1000 MC trials, namely the ratio between the number of misclassified measurements for a given class (target) and the true quantity for that category. Again, the advantage of the proposed method over the considered competitors is quite evident.

Finally, to assess the estimation accuracy for the estimates of  $a_l$  and  $b_l$  at the  $n_{mc}$ th MC trial, which are generally denoted by  $\hat{a}_l(n_{mc})$  and  $\hat{b}_l(n_{mc})$ ,  $l = 1, \dots, L$ , respectively, in Table I we evaluate the Percentage Root Mean Square Error (PRMSE) relative to the true values that is defined as

$$\left\{ \begin{array}{l} \text{PRMSE}_{a_l} = \sqrt{\frac{\sum_{n_{mc}=1}^{N_{mc}} \frac{\min_{l' \in \mathcal{A}} (a_l - \hat{a}_{l'})^2}{N_{mc}}}{|a_l|}} \times \frac{100}{|a_l|}, \\ \text{PRMSE}_{b_l} = \sqrt{\frac{\sum_{n_{mc}=1}^{N_{mc}} \frac{\min_{l' \in \mathcal{A}} (b_l - \hat{b}_{l'})^2}{N_{mc}}}{|b_l|}} \times \frac{100}{|b_l|} \end{array} \right. \quad (39)$$

with  $N_{mc} = 1000$  being the number of MC trials. The table highlights that for targets 3 and 4 the estimate of  $a_l$  gives rise to errors greater than 20% due to the fact that the trajectories of these targets are characterized by intersections with other lines whose angular coefficient is considerably different. The same remark also holds for what concerns the errors related to the estimate of  $b_l$ . Otherwise stated, even though the percentage of correct classification is high, when an error occurs, its value can be high due to line intersections. Nevertheless, such errors can be mitigated by filtering the estimates over several consecutive processed batches of measurements.

<sup>2</sup>Observe that analogous curves are not reported in the other subfigures since the KNN and K-means cannot provide such estimates.

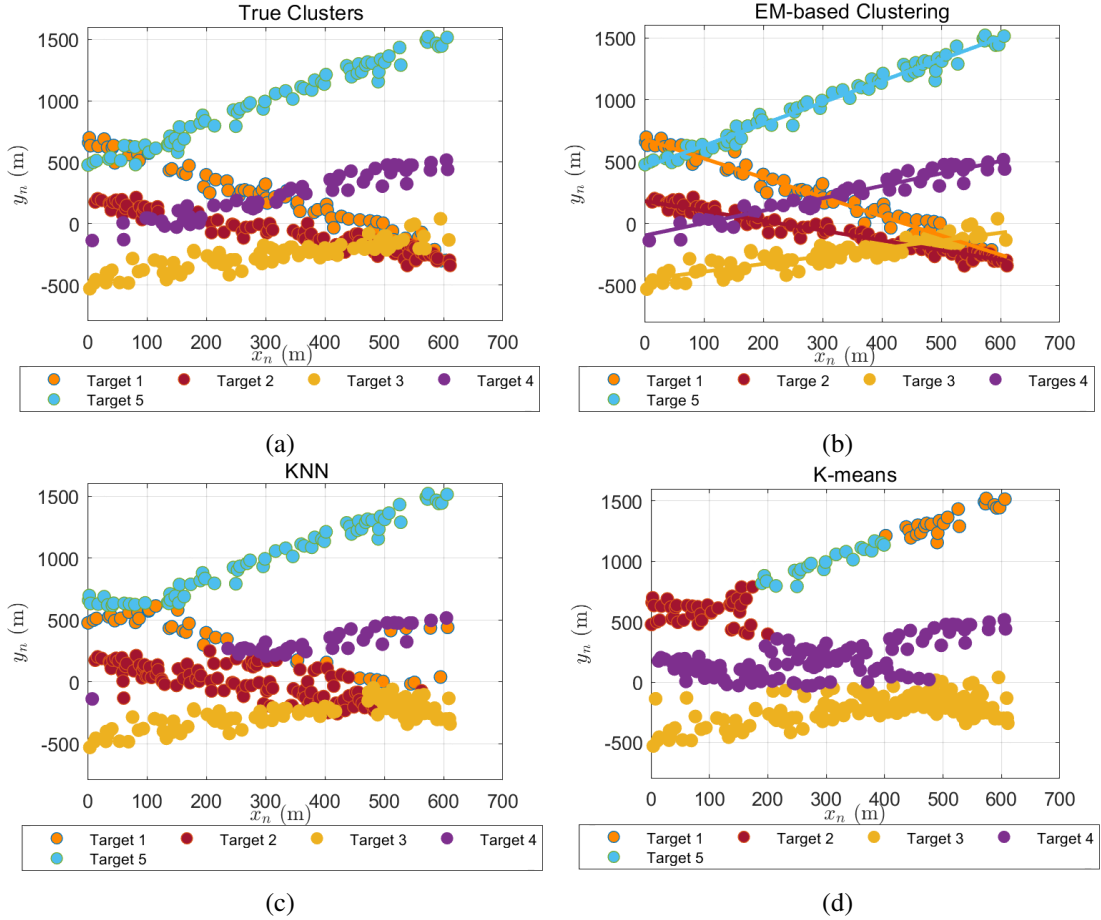


Fig. 4: Cartesian coordinates diagrams for each target over a single MC trial (first scenario): (a) true measurement association; (b) classification (scatter points) results and trajectory fitting (straight lines) for the proposed architecture; (c) classification results for the KNN; (d) classification results for the K-means.

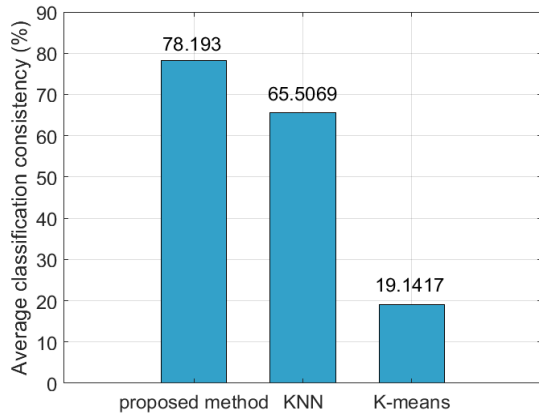


Fig. 5: Average classification consistency (%) over 1000 independent trials for the considered classifiers (first scenario).

TABLE I: PRMSE values (%) for  $a_l$  and  $b_l$ ,  $l = 1, \dots, L$ , over 1000 independent trials (first scenario).

	$l = 1$	$l = 2$	$l = 3$	$l = 4$	$l = 5$
$a_l$	5.3967	17.5596	58.5285	36.8473	1.9468
$b_l$	4.7652	25.8798	13.3593	45.2495	3.1853

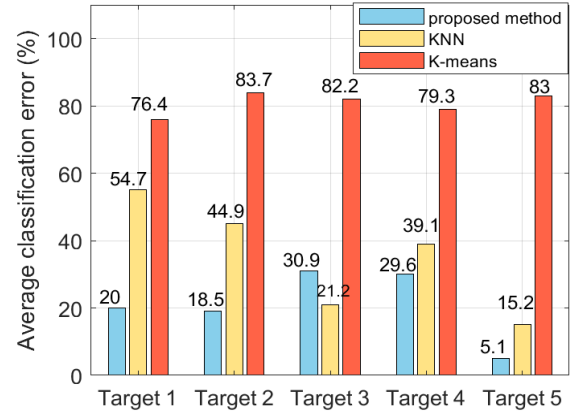


Fig. 6: Average classification error (%) of each target over 1000 independent trials for the considered classifiers (first scenario).

### B. Second Operating Scenario for Known Number of Targets $L = 10$

Now, we consider a more challenging scenario where  $L = 10$  targets are present with different trajectories and



TABLE II: PRMSE values (%) for  $a_l$  and  $b_l$ ,  $l = 1, \dots, L$ , over 1000 independent trials (second scenario).

	$l = 1$	$l = 2$	$l = 3$	$l = 4$	$l = 5$	$l = 6$	$l = 7$	$l = 8$	$l = 9$	$l = 10$
$a_l$	5.1741	1.7061	39.4472	53.9560	23.3503	16.7256	23.4816	21.8546	11.5735	53.5897
$b_l$	0.8867	0.1999	17.5633	28.8967	79.0360	11.5884	10.3934	10.3873	1.0407	5.7240

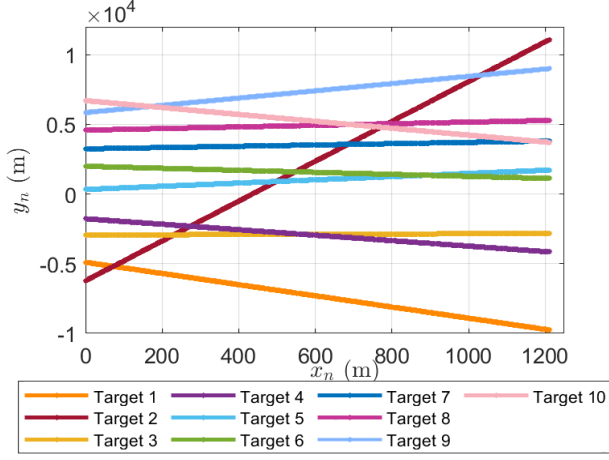
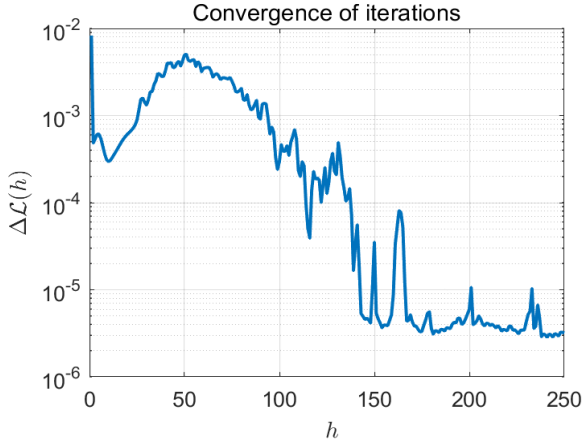


Fig. 7: Clean target trajectories without measurement noise (second scenario).

Fig. 8:  $\Delta\mathcal{L}$  versus  $h$  for the EM-based procedure (second scenario).

intersections. As for the previous case, the KNN and K-means classifiers are taken into account as natural competitors. Target measurements are generated as follows

- **Target 1:**  $y_{n_1}|c_{n_1} = 1 \sim \mathcal{N}(-4.0108x_{n_1} - 4897, \sigma_1^2)$ ,  $n_1 = 1, \dots, N_1$ ;
- **Target 2:**  $y_{n_2}|c_{n_2} = 2 \sim \mathcal{N}(14.3007x_{n_2} - 6230, \sigma_2^2)$ ,  $n_2 = 1, \dots, N_2$ ;
- **Target 3:**  $y_{n_3}|c_{n_3} = 3 \sim \mathcal{N}(0.0875x_{n_3} - 2936, \sigma_3^2)$ ,  $n_3 = 1, \dots, N_3$ ;
- **Target 4:**  $y_{n_4}|c_{n_4} = 4 \sim \mathcal{N}(-1.9626x_{n_4} - 1774, \sigma_4^2)$ ,  $n_4 = 1, \dots, N_4$ ;
- **Target 5:**  $y_{n_5}|c_{n_5} = 5 \sim \mathcal{N}(1.1504x_{n_5} + 330, \sigma_5^2)$ ,  $n_5 = 1, \dots, N_5$ ;
- **Target 6:**  $y_{n_6}|c_{n_6} = 6 \sim \mathcal{N}(-0.7265x_{n_6} + 1997, \sigma_6^2)$ ,  $n_6 = 1, \dots, N_6$ ;
- **Target 7:**  $y_{n_7}|c_{n_7} = 7 \sim \mathcal{N}(0.4663x_{n_7} + 3245, \sigma_7^2)$ ,

$$n_7 = 1, \dots, N_7;$$

- **Target 8:**  $y_{n_8}|c_{n_8} = 8 \sim \mathcal{N}(0.5774x_{n_8} + 4588, \sigma_8^2)$ ,  $n_8 = 1, \dots, N_8$ ;
- **Target 9:**  $y_{n_9}|c_{n_9} = 9 \sim \mathcal{N}(2.6051x_{n_9} + 5846, \sigma_9^2)$ ,  $n_9 = 1, \dots, N_9$ ;
- **Target 10:**  $y_{n_{10}}|c_{n_{10}} = 10 \sim \mathcal{N}(-2.4751x_{n_{10}} + 6706, \sigma_{10}^2)$ ,  $n_{10} = 1, \dots, N_{10}$ .

The number of measurements for each target is generated as in the previous case and the clean trajectories are shown in Figure 7. The classification performances of the proposed architecture are investigated assuming  $h_{max} = 250$ . Such a value is selected from Figure 8 where the relative variation of the log-likelihood is below  $10^{-5}$  for  $h = 250$ .

In Figures 9-11, we provide a qualitative and quantitative assessment of the classification performance for the three algorithms. As observed for the case  $L = 5$ , the EM-based classifier is less inclined to partition the measurement set corresponding to a given target into subsets associated to other targets. This behavior is evident in Figure 9 where the K-means experiences the worst performance corroborating what indicated by Figure 5. Figures 10-11 point out the EM-based method provides an overall performance that is superior with respect to that of the considered competitors, even though for some targets the KNN (that is a supervised method) can return lower classification errors with respect of the EM-based classifier (that is an unsupervised method).

Finally, in Table II, we report the PRMSE for the estimates of  $a_l$  and  $b_l$ ,  $l = 1, \dots, 10$ . In this case, the errors related to  $b_l$  are small except for target 5 whose trajectory intersects that of target 6 maintaining a low separation. As for the errors related to  $a_l$ , the highest values are returned for targets 3, 4, and 10. In fact, the lines corresponding to these targets share an intersection with the line associated to target 2 whose angular coefficient is significantly different from the other.

### C. Operating Scenario where Number of Targets is Unknown

In this section, the classification and estimation performance is assessed when the number of targets is unknown under the constraint  $L_{max} = 10$ . The scenario considered in what follows comprises  $L = 3$  targets whose trajectories are

- **Target 1:**  $y_{n_1}|c_{n_1} = 1 \sim \mathcal{N}(-1.8807x_{n_1} + 771, \sigma_1^2)$ ,  $n_1 = 1, \dots, N_1$ ;
- **Target 2:**  $y_{n_2}|c_{n_2} = 2 \sim \mathcal{N}(-0.2679x_{n_2} + 410, \sigma_2^2)$ ,  $n_2 = 1, \dots, N_2$ ;
- **Target 3:**  $y_{n_3}|c_{n_3} = 3 \sim \mathcal{N}(x_{n_3} - 129, \sigma_3^2)$ ,  $n_3 = 1, \dots, N_3$ ,

More specifically, true clusters with measurement noise variance  $\sigma_l^2 = 50$  and the clean trajectories are shown in Figure 12. Before presenting the estimation results, the convergence rate of the EM procedure over 1000 independent trials using AIC, BIC, and GIC is depicted in Figure 13. The results confirm

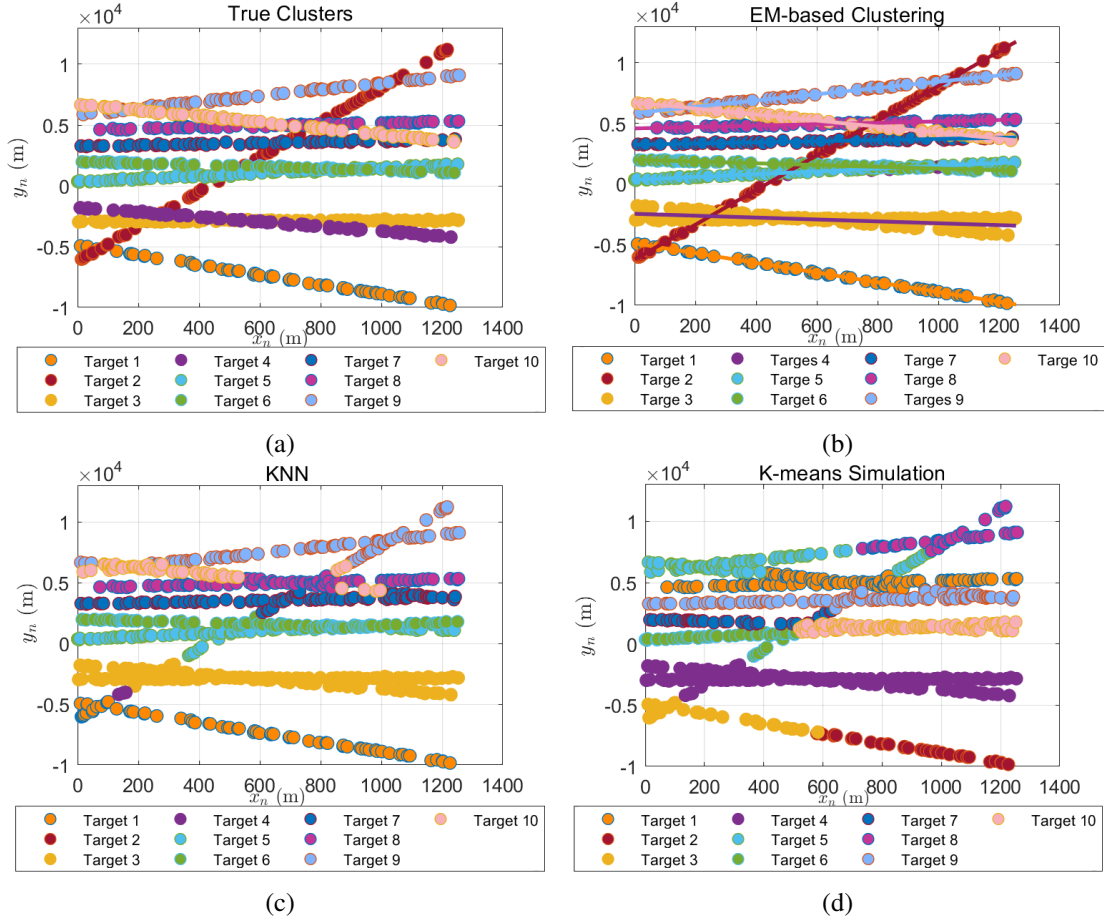


Fig. 9: Scatter diagrams for each target over one trial (second scenario): (a) true measurement association; (b) classification (scatter points) results and trajectory fitting (straight lines) for the proposed architecture; (c) classification results for the KNN; (d) classification results for the K-means.

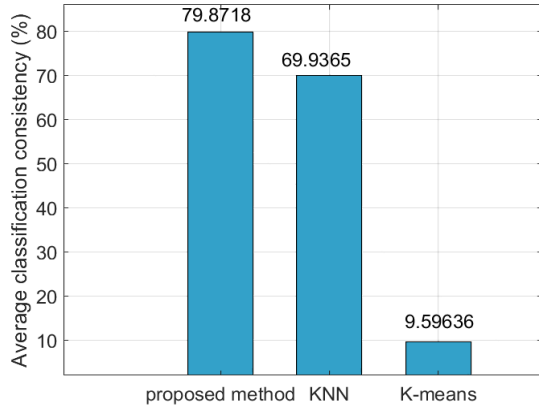


Fig. 10: Average classification consistency (%) over 1000 independent trials (second scenario).

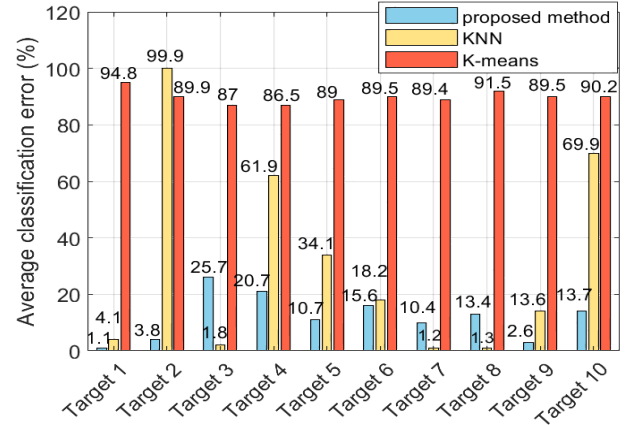


Fig. 11: Average classification error (%) of each target over 1000 independent trials (second scenario).

investigated using the metrics defined in (39) and

that  $h_{max} = 50$  returns a relative variation of  $\Delta\mathcal{L}$  lower than  $10^{-4}$ . The estimation performance related to  $a_l$ ,  $b_l$ , and  $L$  is

$$\text{RMSE}_L = \sqrt{\sum_{n_{mc}=1}^{N_{mc}} (\hat{L}(n_{mc}) - L)^2 / N_{mc}} \quad (40)$$

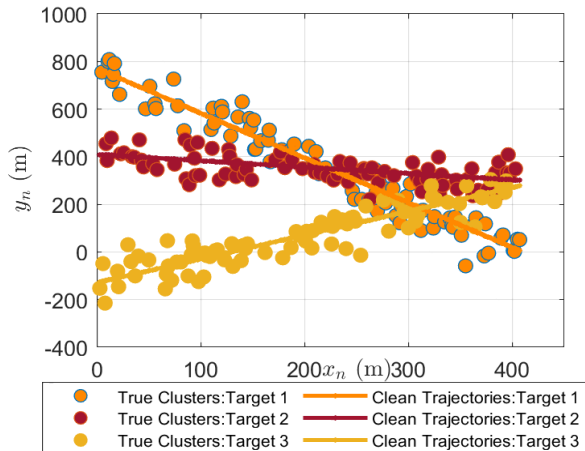


Fig. 12: True clusters and clean trajectories ( $L = 3$ ).

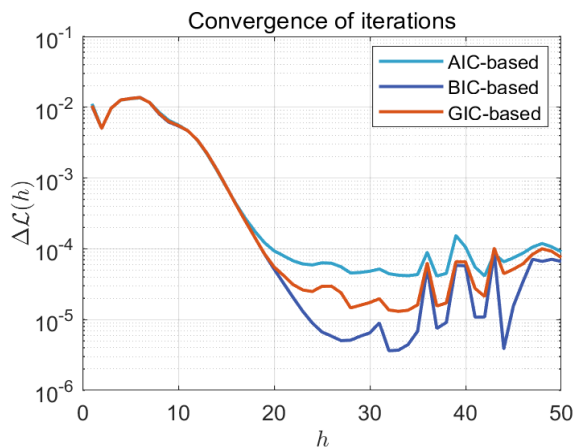


Fig. 13:  $\Delta\mathcal{L}$  versus  $h$  of the EM procedure for the classifiers based on AIC, BIC, and GIC ( $L = 3$ ).

with  $N_{mc} = 1000$ . Table III contains the PRMSE values for what concerns the estimation of the trajectory parameters and points out that the BIC-based clustering architectures provide better results than the classifiers based upon the AIC and GIC. In Figure 14, the RMSE values associated with the estimation of  $L$  confirm the superiority of the BIC-based classifier that returns an error lower than 0.5 at least for the considered parameters.

## VI. CONCLUSIONS AND FUTURE WORKS

In this work, we have proposed a solution for clustering data generated by the nodes of a radar network where each node has limited processing capabilities. In fact, we have assumed that the fusion center collects (2-dimensional) position measurements without any side information that can be used to create clusters associated with the targets in the region of interest. To this end, we have used fictitious nonobservable random variables that represent the label of each measurement. Then, we have estimated the posterior probability that a label takes on a specific value given the corresponding measurement by resorting to the EM-algorithm. The clustering is performed by selecting the label that returns the highest posterior probability.

TABLE III: PRMSE values (%) for  $a_l$  and  $b_l$ ,  $l = 1, \dots, L$ , using AIC, BIC, and GIC over 1000 independent trials ( $L = 3$ ).

		$l = 1$	$l = 2$	$l = 3$
<b>AIC-based</b>	$a_l$	4.1803	30.1187	8.6034
	$b_l$	1.8741	3.7893	11.9821
<b>BIC-based</b>	$a_l$	3.8201	27.1248	7.5070
	$b_l$	1.7480	3.2314	10.1665
<b>GIC-based</b>	$a_l$	3.8727	27.4196	7.7718
	$b_l$	1.7651	3.2885	10.4805

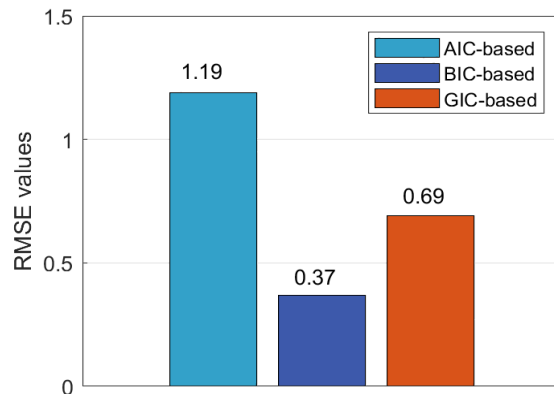


Fig. 14: RMSE values for  $L$  for the classifiers based upon the AIC, BIC, and GIC over 1000 independent trials ( $L = 3$ ).

This method is clearly less time demanding than the plain maximum likelihood approach whose computational load depends on the total number of data partitions as well as the number of targets. The performance assessment has been conducted by using synthetic data and in comparison with well-known data-driven clustering algorithms such as the KNN and K-means. Different challenging scenarios have been considered and for each of them, the proposed algorithm is capable of outperforming the considered competitors for what concerns the clustering and estimation capabilities.

Future research tracks might encompass the extension of the proposed approach to the case where the measurements contain information related to a third-dimension or the target Doppler frequency. The validation of the proposed approach with real recorded data from a radar network is part of the current research activity.

## REFERENCES

- [1] K. Murphy, *Machine Learning: A Probabilistic Perspective*, ser. Adaptive Computation and Machine Learning series. MIT Press, 2012.
- [2] S. Theodoridis, *Machine Learning: A Bayesian and Optimization Perspective*. Elsevier Science, 2015.
- [3] V. S. Chernyak, *Fundamentals of Multisite Radar Systems*. Routledge, 1998.
- [4] G. R. F. Ehlers, D. Orlando, "Batch tracking algorithm for multistatic sonars," *IET Radar, Sonar & Navigation*, vol. 6, pp. 746–752(6), 2012.

- [5] L. Yan, L. Pallotta, G. Giunta, and D. Orlando, "Robust Target Localization for Multistatic Passive Radar Networks," *IEEE Sensors Letters*, vol. 7, no. 7, pp. 1–4, 2023.
- [6] A. Filip and D. Shutin, "Ambiguity function analysis for ofdm-based ldaacs passive multistatic radar," *IEEE Transactions on Aerospace and Electronic Systems*, vol. 54, no. 3, pp. 1323–1340, 2018.
- [7] F. Santi, F. Pieralice, and D. Pastina, "Joint Detection and Localization of Vessels at Sea With a GNSS-Based Multistatic Radar," *IEEE Transactions on Geoscience and Remote Sensing*, vol. 57, no. 8, pp. 5894–5913, 2019.
- [8] J. Liu, H. Li, and B. Himed, "Two Target Detection Algorithms for Passive Multistatic Radar," *IEEE Transactions on Signal Processing*, vol. 62, no. 22, pp. 5930–5939, 2014.
- [9] B. Sobhani, E. Paolini, A. Giorgetti, M. Mazzotti, and M. Chiani, "Target Tracking for UWB Multistatic Radar Sensor Networks," *IEEE Journal of Selected Topics in Signal Processing*, vol. 8, no. 1, pp. 125–136, 2014.
- [10] M. Boutkhil, A. Driouach, and A. Khamlichi, "Detecting and localizing moving targets using multistatic radar system," *Procedia Manufacturing*, vol. 22, pp. 455–462, 2018, 11th International Conference Interdisciplinarity in Engineering, INTER-ENG 2017, 5-6 October 2017, Tirgu Mures, Romania. [Online]. Available: <https://www.sciencedirect.com/science/article/pii/S2351978918303640>
- [11] J. Ma and X. Rui, "Compressive detection of multiple targets in passive bistatic radar," *IET Radar, Sonar & Navigation*, vol. 17, no. 3, pp. 537–544, 2023. [Online]. Available: <https://ietresearch.onlinelibrary.wiley.com/doi/abs/10.1049/rsn2.12358>
- [12] F. Colone, D. W. O'Hagan, P. Lombardo, and C. J. Baker, "A Multistage Processing Algorithm for Disturbance Removal and Target Detection in Passive Bistatic Radar," *IEEE Transactions on Aerospace and Electronic Systems*, vol. 45, no. 2, pp. 698–722, 2009.
- [13] D. Adamy, *EW101: A First Course in Electronic Warfare*, A. House, Ed., Norwood, MA, 2001.
- [14] G. Stimson, H. Griffiths, C. Baker, D. Adamy, and D. Adamy, *Stimson's Introduction to Airborne Radar*, ser. Radar, Sonar and Navigation. SciTech Publishing, 2014.
- [15] S. H. Javadi and A. Farina, "Radar networks: A review of features and challenges," *Information Fusion*, vol. 61, pp. 48–55, 2020. [Online]. Available: <https://www.sciencedirect.com/science/article/pii/S1566253519307535>
- [16] S. H. Javadi, "Decision fusion: Sparse network vs. dense network," in *2016 24th Iranian Conference on Electrical Engineering (ICEE)*, 2016, pp. 1821–1824.
- [17] E. Conte, E. D'Addio, A. Farina, and M. Longo, "Multistatic radar detection: synthesis and comparison of optimum and suboptimum receivers," *IEE Proceedings F (Communications, Radar and Signal Processing)*, vol. 130, pp. 484–494(10), October 1983. [Online]. Available: <https://digital-library.theiet.org/content/journals/10.1049/ip-f-1.1983.0078>
- [18] R. R. Tenney and N. R. Sandell, "Detection with distributed sensors," *IEEE Transactions on Aerospace and Electronic Systems*, vol. AES-17, no. 4, p. 501 – 510, 1981.
- [19] J. Fang and H. Li, "Hyperplane-based vector quantization for distributed estimation in wireless sensor networks," *IEEE Transactions on Information Theory*, vol. 55, no. 12, p. 5682 – 5699, 2009.
- [20] R. Niu, P. K. Varshney, and Q. Cheng, "Distributed detection in a large wireless sensor network," *Information Fusion*, vol. 7, no. 4, pp. 380–394, 2006, special Issue on the Seventh International Conference on Information Fusion-Part I. [Online]. Available: <https://www.sciencedirect.com/science/article/pii/S1566253505000710>
- [21] S. H. Javadi and A. Peiravi, "Fusion of weighted decisions in wireless sensor networks," *IET Wireless Sensor Systems*, vol. 5, no. 2, pp. 97–105, 2015. [Online]. Available: <https://ietresearch.onlinelibrary.wiley.com/doi/abs/10.1049/iet-wss.2013.0116>
- [22] J. Yan, W. Pu, S. Zhou, H. Liu, and Z. Bao, "Collaborative detection and power allocation framework for target tracking in multiple radar system," *Information Fusion*, vol. 55, pp. 173–183, 2020. [Online]. Available: <https://www.sciencedirect.com/science/article/pii/S1566253518301210>
- [23] Y. Bar-Shalom, F. Daum, and J. Huang, "The probabilistic data association filter," *IEEE Control Systems Magazine*, vol. 29, no. 6, pp. 82–100, 2009.
- [24] Y. Bar-Shalom and X.-R. Li, *Multitarget-multisensor tracking: principles and techniques*. YBs Storrs, CT, 1995, vol. 19.
- [25] S. Nannuru, S. Blouin, M. Coates, and M. Rabbat, "Multisensor cphd filter," *IEEE Transactions on Aerospace and Electronic Systems*, vol. 52, no. 4, pp. 1834–1854, 2016.
- [26] X. Yang, W.-A. Zhang, L. Yu, and K. Xing, "Multi-rate distributed fusion estimation for sensor network-based target tracking," *IEEE Sensors Journal*, vol. 16, no. 5, pp. 1233–1242, 2015.
- [27] K.-C. Chang, R. K. Saha, and Y. Bar-Shalom, "On optimal track-to-track fusion," *IEEE Transactions on Aerospace and Electronic Systems*, vol. 33, no. 4, pp. 1271–1276, 1997.
- [28] G. Battistelli, L. Chisci, C. Fantacci, A. Farina, and A. Graziano, "Consensus cphd filter for distributed multitarget tracking," *IEEE Journal of Selected Topics in Signal Processing*, vol. 7, no. 3, pp. 508–520, 2013.
- [29] T. Li, J. Prieto, H. Fan, and J. M. Corchado, "A robust multi-sensor phd filter based on multi-sensor measurement clustering," *IEEE Communications Letters*, vol. 22, no. 10, pp. 2064–2067, 2018.
- [30] A. Coluccia, A. Fascista, and G. Ricci, "CFAR Feature Plane: A Novel Framework for the Analysis and Design of Radar Detectors," *IEEE Transactions on Signal Processing*, vol. 68, pp. 3903–3916, 2020.
- [31] —, "Design of Customized Adaptive Radar Detectors in the CFAR Feature Plane," *IEEE Transactions on Signal Processing*, vol. 70, pp. 5133–5147, 2022.
- [32] L. Scharf and C. Demeure, *Statistical Signal Processing: Detection, Estimation, and Time Series Analysis*, ser. Addison-Wesley series in electrical and computer engineering. Addison-Wesley Publishing Company, 1991.
- [33] P. Addabbo, S. Han, D. Orlando, and G. Ricci, "Learning Strategies for Radar Clutter Classification," *IEEE Transactions on Signal Processing*, vol. 69, pp. 1070–1082, 2021.
- [34] L. Yan, S. Han, C. Hao, D. Orlando, and G. Ricci, "Innovative Cognitive Approaches for Joint Radar Clutter Classification and Multiple Target Detection in Heterogeneous Environments," *IEEE Transactions on Signal Processing*, vol. 71, pp. 1010–1022, 2023.
- [35] A. Coluccia, A. Fascista, D. Orlando, and G. Ricci, "Adaptive Radar Detection in Heterogeneous Clutter Plus Thermal Noise via the Expectation-Maximization Algorithm," *IEEE Transactions on Aerospace and Electronic Systems*, pp. 1–13, 2023.
- [36] S. M. Kay, "The multifamily likelihood ratio test for multiple signal model detection," *IEEE Signal Processing Letters*, vol. 12, no. 5, pp. 369–371, 2005.
- [37] P. Stoica and Y. Selen, "Model-order selection: A review of information criterion rules," *IEEE Signal Processing Magazine*, vol. 21, no. 4, pp. 36–47, 2004.
- [38] A. P. Dempster, N. M. Laird, and D. B. Rubin, "Maximum likelihood from incomplete data via the EM algorithm," *Journal of the Royal Statistical Society (Series B - Methodological)*, vol. 39, no. 1, pp. 1–38, 1977.
- [39] P. Stoica and P. Babu, "On the proper forms of bic for model order selection," *IEEE Transactions on Signal Processing*, vol. 60, no. 9, pp. 4956–4961, September 2012.
- [40] —, "On the exponentially embedded family (eef) rule for model order selection," *IEEE Signal Processing Letters*, vol. 19, no. 9, pp. 551–554, September 2012.
- [41] S. Kay, "Exponentially embedded families-new approaches to model order estimation," *IEEE Trans. on Aerospace and Electronic Systems*, vol. 41, no. 1, pp. 333–345, January 2005.
- [42] S. Han, P. Addabbo, F. Biondi, C. Clemente, D. Orlando, and G. Ricci, "Innovative Solutions Based on the EM-Algorithm for Covariance Structure Detection and Classification in Polarimetric SAR Images," *IEEE Transactions on Aerospace and Electronic Systems*, vol. 59, no. 1, pp. 209–227, 2023.
- [43] C. M. Bishop, *Pattern Recognition and Machine Learning (Information Science and Statistics)*, 1st ed. Springer, 2007.
- [44] S. M. Kay, "The Multifamily Likelihood Ratio Test for Multiple Signal Model Detection," *IEEE Signal Processing Letters*, vol. 12, no. 5, pp. 369–371, May 2005.
- [45] Y. Wang, Z. Pan, and Y. Pan, "A training data set cleaning method by classification ability ranking for the  $k$ -nearest neighbor classifier," *IEEE Transactions on Neural Networks and Learning Systems*, vol. 31, no. 5, pp. 1544–1556, 2020.
- [46] B. Balusamy, N. Abirami R, S. Kadry, and A. H. Gandomi, *Cluster Analysis*, 2021, pp. 259–292.